Hybrid Terahertz Beamforming Relying on Channel Sparsity and Angular Orthogonality

Qingdong Yue, Jie Hu, *Senior Member, IEEE*, Tingyu Shui, Qingxiao Huang, Kun Yang, *Fellow, IEEE*, Lajos Hanzo, *Life Fellow, IEEE*

***Abstract*—As the next generation concepts gravitate towards ultra-high frequency bands, such as the terahertz (THz) band having abundant resources, approaching Tbps transmission rates is becoming a reality. In this contact we may exploit the sparsity of the THz channel, which substantially reduces the hardware complexity, since a single RF chain is capable of designing a near-optimal transmit beamformer in a single-carrier single-user THz system. We then reveal the spatial orthogonality experienced in the downlink of a single-carrier THz broadcast system supporting multiple users. The minimum throughput of the users is maximized by specifically designing the hybrid beamformer. Based on the above-mentioned angular orthogonality, we characterise the asymptotically optimal structure of the hybrid beamformer. Specifically, the asymptotically optimal analog beamformer is represented in closed-form, while its asymptotically optimal digital counterpart is formulated by solving a linear-programming problem. As a special example, the asymptotically optimal hybrid beamformer is also obtained in closed-form for a THz multicast system. Moreover, we obtain the closed-form asymptotically optimal hybrid beamformer of a multi-carrier multi-user system, when we maximize the minimum throughput among all the user. Our numerical results explicitly demonstrate the compelling benefits of our hybrid beamforming design.**

***Index Terms*—Terahertz communication (THz), hybrid beamforming, channel sparsity, spatial orthogonality, low complexity**

I. Introduction

The number of Internet of Things (IoT) devices is expected to grow from about 7 billion in 2018 to 22 billion by 2025 [1], which may lead to a tele-traffic volume up to Tera-bits per seconds in future wireless communications [2]. To support this ultra-high data rate demand, the next generation systems may be expected to harness the Terahertz (THz) band [3], [4] of 0.1-10 THz [5]–[7].

In order to overcome the severe path-loss experienced in THz bands, high-gain multiple-input-multiple-output (MIMO) techniques must be adopted. Thanks to the extremely short wavelength, ultra-massive antennas can be compactly implemented at both the transmitters and receivers for attaining the desired gains [6], [8], [9]. In contrast to the sub-6 GHz band, full-digital transceivers cannot be implemented in the THz bands due to the unaffordable hardware cost and energy consumption [10]. Hence, hybrid beamforming using a limited number of radio-frequency (RF) chains must be conceived [11]–[13]. However, the optimization of their array weights is challenging due to the non-convex constraints imposed on the phase-shifters.

Numerous hybrid beamforming designs have been conceived, especially for the millimeter-wave (mmWave) bands [14]–[17]. As for the connection between RF chains and antennas, both full-connection [18]–[20] and partial-connection architectures have been considered [21], [22]. For the full-connection structure, Zhu *et al.* [18] maximized the achievable sum-rate by jointly optimizing the hybrid beamforming weights and the power allocation, subject to a minimum spectral efficiency constraint on every user. Pang *et al.* [23] considered non-orthogonal multiple access in the downlink of multi-user mmWave systems. In order to maximize the signal-to-interference-plus-noise-ratio (SINR), both the power allocation and the hybrid beamformer weights were jointly designed. Zhan *et al.* [24] proposed an interference cancellation aided hybrid beamformer for the downlink of a mmWave-MIMO system supporting multiple-users. As for the partial-connection based structure , Li *et al.* [21] investigated a wideband mmWave MIMO-OFDM system. A dynamic partial-connection structure, relying on a hybrid transmit beamformer (TBF) and received combiner (RC) were jointly designed by maximizing the average spectral efficiency. Feng *et al.* [22] explored reconfigurable intelligent surface (RIS) aided mmWave communication systems. They maximized the bandwidth-efficiency by optimizing the hybrid TBF relying on a partial-connection aided structure and a passive beamformer constituted by the RIS.

Some recent contributions also conceived hybrid single-carrier TBFs for the THz bands. [6], [19], [20], [25], [26], [26], [27]. Specifically, Lin *et al.* [25] investigated a codebook-based TBF for maximizing the sum-rate of multi-user mWave and THz systems. Moreover, Lin *et al.* [20] investigated a multi-user MIMO-THz system relying on multiple carriers. They jointly designed both the antenna connection structure and the corresponding hybrid TBF for the sake of maximizing the spectral efficiency. Busari *et al.* [26] designed a hybrid TBF for vehicular connectivity in the THz band. Furthermore, Lin *et al.* [27] studied an indoor communication system and

Qingdong Yue, Jie Hu, Qingxiao Huang and Tingyu Shui are with the School of Information and Communication Engineering, University of Electronic Science and Technology of China, Chengdu, 611731, China, email: qdyue1588@163.com, hujie@uestc.edu.cn, grady_ustec@126.com. and 377145470@qq.com

Kun Yang is with the School of Computer Science and Electronic Engineering, University of Essex, Colchester, CO4 3SQ, U.K., email: kunyang@essex.ac.uk.

Lajos Hanzo is with the School of Electronics and Computer Science, University of Southampton, Southampton, SO17 1BJ, U.K., email: lh@ecs.soton.ac.uk.

L. Hanzo would like to acknowledge the financial support of the Engineering and Physical Sciences Research Council projects EP/W016605/1, EP/X01228X/1 and EP/Y026721/1 as well as of the European Research Council's Advanced Fellow Grant QuantCom (Grant No. 789028)

obtained an upper-bound of the ergodic capacity. Qiao *et al.* [28] designed a secure RIS-assisted THz system by jointly optimizing the TBF and the passive RIS-based beamformer to maximize the secrecy rate, subject to specific transmit power constraints and to phase-shifter resolution constraints. Wang *et al.* [29] developed a donwlink beam training method for the cascaded 2-hop transmitter-RIS-user channel in a THz system. Finally, Gao *et al.* [6] eliminated the impact of beam split by inventing a virtual partial-connection technique. Therefore, the spectral efficiency was substantially improved.

The THz band provides abundant spectral resources. Some authors focus on the multi-carrier TBF designs for the THz bands [6], [19], [30], [31]. Due to the non-negligible molecular absorption loss, THz channels have high distance and frequency dependence [19]. Yuan *et al.* [19] designed a hybrid TBF for multi-carrier MIMO-THz systems communicating over frequency-selective fading channels. Yuan *et al.* [31] also designed a TBF for a cluster-based multi-carrier beam division multiple access scheme. Moreover, large bandwidth and large number of antennas in THz results in the phenomenon of beam split [6]. To solve this problem, Gao *et al.* [6] designed a true time delay based TBF for multi-carrier systems to maximize the achievable rate. Yan *et al.* [30] designed a dynamic-subarray relying upon a fixed true time delay architecture in multi-carrier THz system. They maximized the achievable rate by optimizing the antenna structure, the TBF and the phase in true time delay.

However, the existing hybrid beamforming designs conceived for THz communication systems have the following drawbacks:

- None of them exploits the spatial orthogonality of THz channels in their beamformer design. Furthermore, there is a paucity of treatises on the characterization of THz communication.
- Typically, semi-definite-relaxation (SDR) and alternative optimisation (AO) are adopted for the transmit beamforming design of large-scale antenna array aided single carrier communication systems, which constitute a fundamental semi-definite-programming (SDP) framework. However, this imposes an excessive computational complexity.
- In multi-carrier systems, typically a true time delay hybrid beamforming architecture is employed for improving the communication performance. However, this introduces time delay and ignores the spatial orthogonality of THz channels, which results in high hardware complexity.

Against this background, our novel contributions are boldly and explicitly contrasted to the literature in TABLE I and are summarized as followings:

- We investigate the downlink of a THz communication system supporting a single user, while exploiting the channel sparsity. A near-optimal THz TBF is designed by only adjusting the phases of the transmit signals in the analog domain with the aid of a single RF chain. By contrast, in the mmWave band, the number of the RF chains should be equal to that of the transmission paths in order to approach the beamformer's optimal performance.
- The spatial orthogonality is rigorously characterised in the angular domain of THz bands, with special emphasis on the downlink of THz single-carrier broadcast systems supporting multiple users. We maximize the minimum achievable rate among all the users by specifically designing the hybrid TBF, subject to the particular power budget and norm constrains of the phase-shifters. By exploiting the angular orthogonality of the users, we characterise the asymptotically optimal structure of the hybrid TBF. Furthermore, the asymptotically optimal analog TBF is then expressed in closed form, while the asymptotically optimal digital TBF is found by solving a linear-programming problem. The resultant computational complexity is far lower than that of its SDP based counterpart. As a specific example, the asymptotically optimal hybrid TBF of a THz single-carrier multicast system is derived in closed form by exploiting the angular orthogonality of the users for maximizing the achievable multicast downlink rate.
- In the multi-carrier systems, we consider molecular absorption loss in THz channels and solve the beam split problem in the digital domian of the hybrid TBF, which performs better than the true-time-delay based TBF. We propose a bisection aided search algorithm for the multi-carrier multi-user system to obtain the asymptotically optimal hybrid beamformer, when we maximize the minimum throughput among all the user. We obtain the closed-form asymptotically optimal analog TBF by extending the angular orthogonality to a multi-carrier system in THz. We obtain the closed-form asymptotically optimal digital TBF having a fixed throughput, while the optimal throughput is obtained by a one-dimensional bisection based search.

The rest of the paper is organised as follows: After studying the single user THz system in Section II, we characterise the spatial orthogonality of the THz band and investigate our multi-user system in Section III. Then we explore a multi-carrier THz system in Section IV. Our numerical results are presented in Section V, following our conclusions in Section VI.

Notation: $(\cdot)^H$ denotes conjugate transpose operations; $\mathbb{E}\{\cdot\}$ represents the statistical expectation; $|a|$ and $\|\mathbf{a}\|$ are the magnitude and norm of a scalar a and vector $\mathbf{a}$; $\|\mathbf{A}\|$ denotes the Frobenius norm of the matrix $\mathbf{A}$; $\mathbf{A}(i, j)$ represents the specific element in the i-th row and j-th column of $\mathbf{A}$; $diag(\mathbf{a})$ is the vector $\mathbf{a}$ diagonalized to a diagonal matrix. Other notations are listed in TABLE II for the sake of clarity.

II. Hybrid Beamforming Design in Single Carrier Single User System

A. System Model

Our system consists of a pair of downlink transmitter and receiver. The user is equipped with a single receive antenna (RA), while the transmitter is equipped with a very large number of N_t of transmit antennas (TAs). The transmitter sends a modulated symbol s to the user, where $s \sim \mathcal{CN}(0, 1)$ is a random complex scalar. The transmit signal is then expressed

TABLE I
SUMMARY OF LITERATURE SURVEY ON HYBRID BEAMFORMING (H: HIGH, ASY-O: ASYMPTOTICALLY OPTIMAL, SC: SINGLE-CARRIER, MC: MULTI-CARRIER)

	[24]	[26]	[25]	[19]	[20]	[28]	[32]	[33]	[6]	[30]	Proposed
THz Bands			✓	✓	✓	✓	✓	✓	✓	✓	✓
Hybrid Beamforming	✓	✓	✓	✓	✓	✓	✓	✓	✓	✓	✓
Exploring Spatial Orthogonality											✓
Optimality											ASY-O
Complexity	$O(KN_t)$	H	H	$O(\|\mathcal{M}\|M^2N_t$ $+\|\mathcal{M}\|M^3)$	$O(N_t^3)$	H	H	H	H	$O(I\|\mathcal{M}\|M^2N_t)$	SC: $O(N_tK+\log_2(1/\varepsilon)I_0K^{2.5})$ MC: $O(N_tK+I_1I_2\|\mathcal{M}\|^2)$
Multi-carrier				✓	✓				✓	✓	✓
Considering spectrum windows			✓	✓	✓		✓	✓		✓	✓
Considering beam split									✓	✓	✓

TABLE II
LIST OF NOTATION

Notations	Explanations
α	The channel's fading coefficient
β	The channel's path-loss coefficient
τ	The channel's time-delay
θ	The departure azimuth angle
ϕ	The departure elevation angle
$\mathbf{a}_t(\theta,\phi)$	The transmit response vectors
$\mathbf{h}_k$	The channel gain from the transmitter to user k
N_t	The number of transmit antennas
P_T	The maximum transmit power
$\mathbf{R}_k$	The achievable rate of user k
$\mathbf{F}_{RF}$	The passband analog beamformer
$\mathbf{F}_{BB}$	The baseband digital beamformer
$P_{I,(i,k)}$	The interference of the i-th information flow imposed on user k
$\mathcal{M}_k$	The set of sub-carriers allocated to user k

as $\mathbf{x} = \mathbf{f}s$, where $\mathbf{f}$ represents the transmit beamformer. The signal received by the user is expressed as

$$y = \sqrt{P_t}\mathbf{h}\mathbf{f}s + n, \tag{1}$$

where the complex random scalar $n \sim \mathcal{CN}(0,\sigma^2)$ represents the noise at the user and the $N_t \times 1$ complex vector $\mathbf{h}$ hosts the channel coefficients of the link directed at the user, where P_t is the maximum transmit power.

B. Channel Model

The channel model is reformulated as

$$\mathbf{h} = \alpha^{[0]}\beta^{[0]}\mathbf{a}_t(\theta^{[0]},\phi^{[0]}) + \sum_{i=1}^{L}\alpha^{[i]}\beta^{[i]}\mathbf{a}_t(\theta^{[i]},\phi^{[i]}), \tag{2}$$

where the first term is the line of sight (LoS) component and the second summation term is the non-LoS (NLoS) component, as shown in Fig. 1. Specifically, $\alpha^{[0]}$ and $\beta^{[0]}$ represent the channel's fading coefficient and the path-loss coefficient of the LoS component, respectively. The NLoS component has L different propagation paths, while $\alpha^{[i]}$ and $\beta^{[i]}$ represent the channel's fading coefficient and the path-loss coefficient of the i-th path. Moreover, $\{\mathbf{a}_t(\theta^{[i]},\phi^{[i]}) \in \mathbb{C}^{N_t\times 1} | i = 0,1,\cdots,L\}$ are the corresponding transmit response vectors, which are

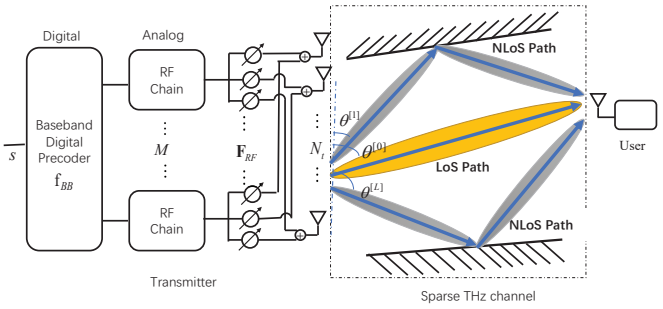

Fig. 1. A single user communication system with a hybrid beaforming architecture.

determined by the structure of the TA arrays as well as the azimuth angles $\theta^{[i]}$ and the elevation angles $\phi^{[i]}$, respectively. When a uniform planar array W and H antennas on the y and z axes is used in the yz-plane[2], respectively, the channel response vector $\mathbf{a}_t(\theta^{[i]},\phi^{[i]})$ is expressed as

$$\mathbf{a}_t(\theta^{[i]},\phi^{[i]}) = \frac{1}{\sqrt{N_t}}[1,\cdots,e^{j\frac{2\pi}{\lambda}d(m\sin(\theta^{[i]})\sin(\phi^{[i]})+n\cos(\phi^{[i]}))},\cdots, e^{j\frac{2\pi}{\lambda}d((W-1)\sin(\theta^{[i]})\sin(\phi^{[i]})+(H-1)\cos(\phi^{[i]}))}], \tag{3}$$

where λ is the wavelength and d is the distance between two adjacent antennas. Furthermore, $0 \le m < W$ and $0 \le n < H$ are the indices of an antenna elements in y- and z- axes, respectively, while the size of the antenna array is $N_t = WH$.

C. Near-optimal Beamformer

It is widely exploited that the maximum-ratio TBF $\mathbf{f}^* = \mathbf{h}^H/\|\mathbf{h}\|$ is optimal. However, it requires a full-digital architecture at the transmitter to achieve optimality, which is unaffordable for large-scale antenna-arrays. Therefore, typically hybrid TBFs are adopted in the mmWave and THz bands. We assume that the transmitter is equipped with M RF chains, as shown in Fig. 1. The baseband digital TBF $\mathbf{f}_{BB} \in \mathbb{C}^{M\times 1}$ forwards the modulated symbols s to M RF chains. Then the up converted passband analog beamformer $\mathbf{F}_{RF} \in \mathbb{C}^{N_t\times M}$ further up converts and forwards the output of the M RF chains to the N_t antennas for transmission. Every RF chain is connected to all the N_t TAs via N_t analog phase-shifters, which results in a fully-

connected topology between the RF chain and the TAs. Note that the analog TBF is constituted by a number of analog phase-shifters satisfying $\|\mathbf{F}_{RF}(i,j)\| = 1, \forall i, \forall j$. In order to construct the optimal TBF, we should let $\mathbf{F}_{RF}\mathbf{f}_{BB} = \mathbf{f}^*$.

In the mmWave channel, the NLoS component is as important as the LoS component, as expressed in Eq. (2). The optimal TBF is formulated as

$$\mathbf{f}_{mmW} = \frac{\mathbf{h}^H}{\|\mathbf{h}\|} = \frac{\sum_{i=0}^{L} \alpha_i \beta_i \mathbf{a}_t(\theta^{[i]}, \phi^{[i]})}{\|\sum_{i=0}^{L} \alpha_i \beta_i \mathbf{a}_t(\theta^{[i]}, \phi^{[i]})\|}. \tag{4}$$

Again, for the of hybrid TBF, we have $\mathbf{f}_{mmW} = \mathbf{F}_{RF}\mathbf{f}_{BB}$. Therefore, we have the following proposition.

Proposition 1: The optimal analog TBF $\mathbf{F}_{RF}$ and the digital TBF $\mathbf{f}_{BB}$ of a mmWave channel are expressed as

$$\begin{aligned} \mathbf{F}_{RF} &= [\mathbf{a}_t(\theta^{[0]}, \phi^{[0]}), \mathbf{a}_t(\theta^{[1]}, \phi^{[1]}), \cdots, \mathbf{a}_t(\theta^{[L]}, \phi^{[L]})], \\ \mathbf{f}_{BB} &= [\alpha_0\beta_0, \alpha_1\beta_1 \cdots, \alpha_L\beta_L]/\|\mathbf{h}\|. \end{aligned} \tag{5}$$

Remark 1: To implement this hybrid TBF, the transmitter has to simultaneously adjust the amplitude in the digital domain and the phase in the analog domain. Moreover, observe from Eq. (5) that in order to achieve optimality, the transmitter needs $M = (L+1)$ RF chains for adjusting the amplitude of the transmit signals in all the $(L+1)$ paths, while we also need a full-connection topology between the RF chains and the antennas. Specifically, the amplitude of the i-th RF chain is set to $\alpha_i\beta_i/\|\mathbf{h}\|$, while its corresponding phase-adjustment in the analog domain is set to $\mathbf{a}_t(\theta^{[i]}, \phi^{[i]})$. Since this hybrid TBF uses as many RF chains as the number of channel paths to fully utilize both the LoS and NLoS componets, Eq. (5) is also the optimal THz TBF when NLoS components are considered.

By contrast, since the wavelength of THz signals is comparable to surface sizes, the surfaces are rough in THz bands. Due to the reflection coefficient of NLoS components is related to the Rayleigh roughness factor, the path-loss coefficient β_0 of the LoS component is far lower than $\{\beta_1, \beta_2, \cdots, \beta_L\}$ of all the NLoS components in the THz bands [20]. Therefore, we have the following proposition.

Proposition 2: The near-optimal THz TBF is reformulated as

$$\mathbf{f}_{THz} = \frac{\mathbf{h}^H}{\|\mathbf{h}\|} \approx \mathbf{a}_t(\theta^{[0]}, \phi^{[0]}). \tag{6}$$

The corresponding analog TBF obeys $\mathbf{f}_{RF} = \mathbf{a}_t(\theta^{[0]}, \phi^{[0]})$ and the digital TBF obeys $f_{BB} = 1$, since $\mathbf{f}_{THz} = \mathbf{f}_{RF} f_{BB}$.

Remark 2: Eq. (6) indicates that we only have to adjust the phase of the transmit signals in the analog domain to construct the near-optimal TBF $\mathbf{f}_{THz}$. Since we do not need any amplitude adjustment, only a single RF chain $M = 1$ is required for approaching optimality. By exploiting the THz channel's sparsity, the hardware complexity can be substantially reduced.

III. Hybrid Beamforming Design for Single Carrier Multi-user Broadcast Systems

A. Multi-user System Model

As portrayed in Fig. 2, the system consists of a single transmitter and K users. All the users are equipped with a single RA, while the transmitter is equipped with a very large number N_t of TAs. Moreover, K RF chains are used at the transmitter, which satisfies $1 \le K \le N_t$. The transmitter sends a range of modulated symbols $\mathbf{s} = [s_1, s_2, \cdots, s_K]$ to all the users, where $s_k \sim \mathcal{CN}(0,1)$ is a random complex scalar requested by the k-th user. As shown in Fig. 2, the baseband digital TBF $\mathbf{F}_{BB} \in \mathbb{C}^{K\times K}$ converts the K modulated symbols to K RF chains. Then the passband analog TBF $\mathbf{F}_{RF} \in \mathbb{C}^{N_t\times K}$ forwards the output of the K RF chains to the N_t TAs for transmission. A full-connection topology is used between the RF chains and the TAs. Note that the analog TBF is constituted by a number of analog phase-shifters satisfying $\|\mathbf{F}_{RF}(i,j)\| = 1, \forall i, \forall j$. The transmit signal is then expressed as $\mathbf{x} = \mathbf{F_{RF}}\mathbf{F_{BB}}\mathbf{s}$. The signal received by the k-th user is obtained as

$$\begin{aligned} y_k &= \mathbf{h}_k\mathbf{F}_{RF}\mathbf{F}_{BB}\mathbf{s} + n_k, \\ &= \underbrace{\mathbf{h}_k\mathbf{F}_{RF}\mathbf{F}_{BB}[k,:]s_k}_{\text{desired signal}} + \underbrace{\sum_{i\neq k} \mathbf{h}_k\mathbf{F}_{RF}\mathbf{F}_{BB}[i,:]s_i}_{\text{interference}} + n_k, \end{aligned} \tag{7}$$

for $\forall k = 1, 2, \cdots, K$, where the random complex scalar $n_k \sim \mathcal{CN}(0, \sigma^2)$ represents the noise at the user and the $N_t \times 1$ complex vector $\mathbf{h}_k$ is the channel directed towards the k-th user. Moreover, P_t is the maximum transmit power.

Based on the received signal of the k-th user expressed in Eq.(7), the SINR of the k-th user is formulated as

$$\gamma_k = \frac{\|\mathbf{h}_k\mathbf{F_{RF}}\mathbf{F_{BB}}[:,k]\|^2}{\|\sum_{i\neq k} \mathbf{h}_k\mathbf{F_{RF}}\mathbf{F_{BB}}[:,i]\|^2 + \sigma^2}. \tag{8}$$

The achievable rate of the k-th user is expressed as

$$R_k = \log_2(1 + \gamma_k). \tag{9}$$

B. Angular Orthogonality of the Users

If the system has $K > 1$ users, angular orthogonality may be arranged between any pair of users.

Lemma 1: Given an infinite number of TAs, the channel's response vectors $\mathbf{h}_k$ and $\mathbf{h}_{k'}$ having different departure azimuth angles satisfy the following equalities:

$$\begin{cases} \lim_{N_t\to\infty} \mathbf{a}_t(\theta_k^{[0]}, \phi_k^{[0]})\mathbf{a}_t(\theta_k^{[0]}, \phi_k^{[0]})^H = 1, \\ \lim_{N_t\to\infty} \mathbf{a}_t(\theta_k^{[0]}, \phi_k^{[0]})\mathbf{a}_t(\theta_{k'}^{[0]}, \phi_{k'}^{[0]})^H = 0, \end{cases} \tag{10}$$

where θ_k (ϕ_k) and $\theta_{k'}$ ($\phi_{k'}$) are the departure azimuth (elevation) angles in the LoS component in $\mathbf{h}_k$ and $\mathbf{h}_{k'}$, respectively.

Proof: Please refer to Appendix A. ■

Theorem 1: Angular orthogonality in THz bands. Let $\mathbf{h}_k$ and $\mathbf{h}_{k'}$ represent the channel spanning from the transmitter to two users, respectively. When we have an infinite number of TAs, these two channels are orthogonal to each other, which is expressed as

$$\lim_{N_t\to\infty} \frac{\mathbf{h}_k\mathbf{h}_{k'}}{N_t} = 0. \tag{11}$$

Proof: The channels $\mathbf{h}_k$ and $\mathbf{h}_{k'}$ from the transmitter to

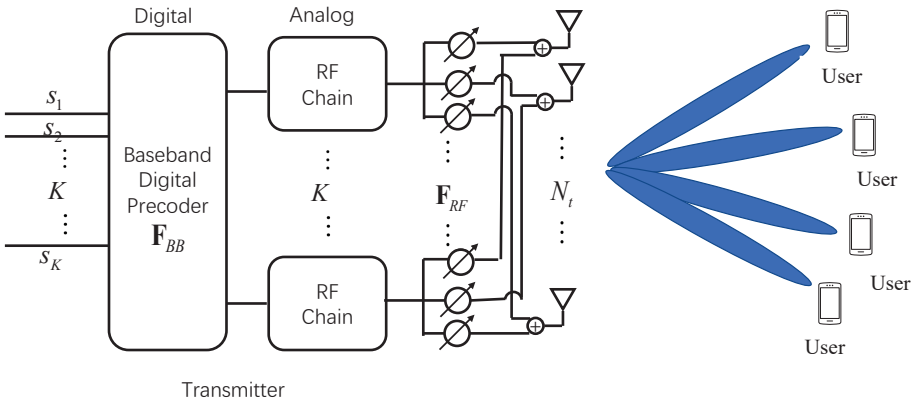

Fig. 2. A downlink communication system in THz bands with a hybrid beamforming architecture.

two users are expressed as

$$\mathbf{h}_k = \alpha_k^{[0]}\beta_k^{[0]}\mathbf{a}_t(\theta_k^{[0]},\phi_k^{[0]}) + \sum_{i=1}^{L}\alpha_k^{[i]}\beta_k^{[i]}\mathbf{a}_t(\theta_k^{[i]},\phi_k^{[0]}), \tag{12}$$

$$\mathbf{h}_{k'} = \alpha_{k'}^{[0]}\beta_{k'}^{[0]}\mathbf{a}_t(\theta_{k'}^{[0]},\phi_{k'}^{[0]}) + \sum_{i=1}^{L}\alpha_{k'}^{[i]}\beta_{k'}^{[i]}\mathbf{a}_t(\theta_{k'}^{[i]},\phi_{k'}^{[0]}),$$

respectively. According to *Lemma 1*, we have

$$\begin{aligned}
\lim_{N_t\to\infty}\frac{\mathbf{h}_k\mathbf{h}_{k'}^H}{N_t} &= \frac{\{\alpha_k^{[0]}\beta_k^{[0]}\mathbf{a}_t(\theta_k^{[0]},\phi_k^{[0]}) + \sum_{i=1}^{L}\alpha_k^{[i]}\beta_k^{[i]}\mathbf{a}_t(\theta_k^{[i]},\phi_k^{[i]})\}}{N_t} \\
&\times\{\alpha_{k'}^{[0]}\beta_{k'}^{[0]}\mathbf{a}_t(\theta_{k'}^{[0]},\phi_{k'}^{[0]}) + \sum_{j=1}^{L}\alpha_{k'}^{[j]}\beta_{k'}^{[j]}\mathbf{a}_t(\theta_{k'}^{[j]},\phi_{k'}^{[j]})\}^H \\
=&\frac{\alpha_k^{[0]}\beta_k^{[0]}(\alpha_{k'}^{[0]}\beta_{k'}^{[0]})^H\mathbf{a}_t(\theta_k^{[0]},\phi_k^{[0]})\mathbf{a}_t(\theta_{k'}^{[0]},\phi_{k'}^{[0]})^H}{N_t} \\
&+\frac{\sum_{i=1}^{L}\alpha_k^{[i]}\beta_k^{[i]}(\alpha_{k'}^{[0]}\beta_{k'}^{[0]})^H\mathbf{a}_t(\theta_k^{[i]},\phi_k^{[i]})\mathbf{a}_t(\theta_{k'}^{[0]},\phi_{k'}^{[0]})^H}{N_t} \\
&+\frac{\sum_{j=1}^{L}\alpha_k^{[0]}\beta_k^{[0]}(\alpha_{k'}^{[j]}\beta_{k'}^{[j]})^H\mathbf{a}_t(\theta_k^{[0]},\phi_k^{[0]})\mathbf{a}_t(\theta_{k'}^{[j]},\phi_{k'}^{[j]})^H}{N_t} \\
&+\frac{\sum_{i=1}^{L}\sum_{j=1}^{L}\alpha_k^{[i]}\beta_k^{[i]}(\alpha_{k'}^{[j]}\beta_{k'}^{[j]})^H\mathbf{a}_t(\theta_k^{[i]},\phi_k^{[i]})\mathbf{a}_t(\theta_{k'}^{[j]},\phi_{k'}^{[j]})^H}{N_t} \\
=&0.
\end{aligned} \tag{13}$$

The proof is completed. ■

Remark 3: Theorem 1 is different from the well-known orthogonality found in massive MIMO systems [34]. The orthogonality in [34] is caused by the rich scattering in the physical environment. It is exploited by random matrix theory and based on the statistical properties of Rayleigh channels. Our proposed theorem relies on the angular domain. The orthogonality is caused by the narrow range of beams associated with large number of antennas.

We investigate the angular orthogonality in Fig 3. We set all the departure elevation angle ϕ fixed as $\pi/2$ and analyze with changing azimuth angle θ. We set the angle of departure (AoD) of the channel response vector towards one user to $\pi/2$, while we generate another channel response vector towards a different user with an AoD ranging from 0 to π. The number

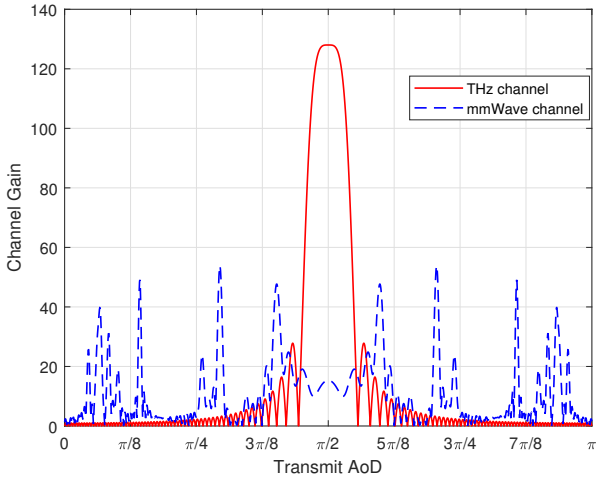

Fig. 3. Angular orthogonality in THz channel.

of TAs is set to $N_t = 128$, while every user is equipped with a single RA. The number of paths in Eq. (2) is set to 3 [20]. The path-loss of the NLoS component is 20 dB higher than that of the LoS component in Eq. (2) [20]. Observe from Fig. 3 that we obtain the maximum inner product of the two channel response vectors when the AoDs of these channels are the same. When the transmit AoD tracks the LoS path, the maximum spatial gain is obtained. Furthermore, there only exists a single peak in THz when we change the transmit AoD, since the spatial gain mainly comes from the LoS path, which also confirms the spatial sparsity. By contrast, observe from Fig. 3 that there exist multiple inner-product peaks in the mmWave band, since the NLoS paths cannot be ignored.

Remark 4: We assume that the THz channel contains a strong LoS path [20]. In *Theorem 1*, we prove the angular orthogonality of THz bands, in which the NLoS components are also considered. In Fig 3 we investigate both the angular orthogonality and the impact of the NLoS and LoS paths. Observe from both the mathematical proof and the simulation results, that statistically the NLoS components have little

impact on the spatial gain. Thus we may simplify the THz TBF design by exploiting *Theorem 1*.

C. Problem Formulation

In order to ensure fairness among all the users, we aim for maximizing the minimum per-user achievable rate of the multi-user system by jointly optimising the digital TBF $\mathbf{F}_{BB}$ and the analog TBF $\mathbf{F}_{RF}$. The corresponding optimisation problem is formulated as

$$\text{(P1)}: \max_{\mathbf{F}_{BB},\mathbf{F}_{RF}} \min_{1\le k\le K} R_k, \tag{14}$$

$$\text{s. t. } ||\mathbf{F}_{BB}\mathbf{F}_{RF}||^2 = 1, \tag{14a}$$

$$||\mathbf{F}_{RF}[i,j]||^2 = P_t, \forall i,j, \tag{14b}$$

where Eq. (14a) represents the transmit power constraint of hybrid TBF, while P_t is the maximum transmit power. Eq. (14b) indicates that the analog TBF $\mathbf{F}_{RF}$ cannot change the amplitudes for the signals.

Proposition 3: The asymptotically optimal analog TBF is $\mathbf{F}^*_{RF} = [\mathbf{a}_t(\theta_1^{[0]},\phi_1^{[0]})^H, \mathbf{a}_t(\theta_2^{[0]},\phi_2^{[0]})^H, \cdots, \mathbf{a}_t(\theta_K^{[0]},\phi_K^{[0]})^H]$, where $\mathbf{a}_t(\theta_k^{[0]},\phi_k^{[0]})$ is the channel response vector in the LoS path directed towards the k-th user and $\theta_k^{[0]}$ ($\phi_k^{[0]}$) is the departure azimuth (elevation) angle in this path.

Proof 1: Please refer to Appendix B.

According to *Proposition 3*, the asymptotically optimal analog TBF $\mathbf{F}^*_{RF}$ only depends on the departure azimuth angle $\{\theta_1^{[0]},\theta_2^{[0]},\cdots,\theta_K^{[0]}\}$ and elevation angle $\{\phi_1^{[0]},\phi_2^{[0]},\cdots,\phi_K^{[0]}\}$. We do not need full channel state information (CSI) for designing the analog TBF. Furthermore, based on the asymptotically optimal analog TBF $\mathbf{F}^*_{RF}$, we have the following proposition for deriving the asymptotically digital TBF $\mathbf{F}^*_{BB}$.

Proposition 4: Given the asymptotically optimal analog TBF $\mathbf{F}^*_{RF}$, the corresponding asymptotically optimal digital TBF $\mathbf{F}^*_{BB}$ is represented by a diagonal matrix.

Proof: Please refer to Appendix C. ∎

By considering both *Propositions 3* and *4*, the SINR γ_k of the k-th user is expressed as

$$\lim_{N_t\to\infty}\gamma_k = \frac{P_t||\mathbf{h}_k\mathbf{F}_{RF}\mathbf{F}_{BB}[:,k]||^2}{P_t\sum_{i\neq k}||\mathbf{h}_k\mathbf{F}_{RF}\mathbf{F}_{BB}[:,i]||^2+\sigma^2} \tag{15}$$

$$= \frac{P_tN_t||\alpha_k^{[0]}\beta_k^{[0]}\mathbf{h}_k\mathbf{a}_t(\theta_k^{[0]})^H\mathbf{F}_{BB}[k,k]||^2}{P_t\sum_{i\neq k}||\alpha_k^{[0]}\beta_k^{[0]}\mathbf{h}_k\mathbf{a}_t(\theta_i^{[0]})^H\mathbf{F}_{BB}[i,i]||^2+\sigma^2} \tag{15a}$$

$$= \frac{P_tN_t||\alpha_k^{[0]}\beta_k^{[0]}\mathbf{F}_{BB}[k,k]||^2}{\sum_{i\neq k}P_{I,(i,k)}||\mathbf{F}_{BB}[i,i]||^2+\sigma^2}, \tag{15b}$$

where we define the interference of the i-th information flow imposed on the k-th user as $P_{I,(i,k)} = ||\alpha_k^{[0]}\beta_k^{[0]}\csc(m\pi(\sin(\theta_k^{[0]})\sin(\phi_k^{[0]})-\sin(\theta_{k'}^{[0]})\sin(\phi_{k'}^{[0]}))+n\pi(\cos(\phi_k^{[0]})-\cos(\phi_{k'}^{[0]})))||^2$. Eq. (15a) is obtained by substituting the asymptotically optimal analog TBF $\mathbf{F}^*_{RF}$ of *Proposition 3* and the diagonal structure of the digital TBF $\mathbf{F}^*_{BB}$ of *Proposition 4* into Eq. (15), while Eq. (15b) is obtained by exploiting the angular orthogonality of *Theorem 1* and *Lemma 1* in Eq. (15a)

Moreover, the asymptotically optimal digital TBF $\mathbf{F}^*_{BB}$ has the following property.

Proposition 5: Given the asymptotically optimal analog TBF $\mathbf{F}^*_{RF}$ in *Proposition 3* and the diagonal structure of the digital TBF $\mathbf{F}^*_{BB}$ in *Proposition 4*, the asymptotically optimal solution of $\mathbf{F}^*_{BB}$ is obtained by guaranteeing that all the users have the same SINR.

Proof: Please refer to Appendix D. ∎

Based on *Propositions 3 - 5*, the asymptotically optimal digital TBF $\mathbf{F}^*_{BB}$ is obtained by the following equation

$$\begin{cases}\gamma_k = \gamma_{k'},\ \forall k,k' \in \{1,2,\cdots,K\}\\ ||\mathbf{F}^*_{BB}\mathbf{F}^*_{RF}||^2 = P_t.\end{cases} \tag{16}$$

Let us set the SINR of all the users equal to a constant as $\{\gamma_k = \gamma_0 | \forall k \in \{1,2,\cdots,K\}\}$.

According to *Proposition 4*, the asymptotically optimal digital TBF $\mathbf{F}^*_{BB}$ should have the following form

$$\mathbf{F}^*_{BB} = diag(\mathbf{F}^*_{BB}[1,1],\cdots\mathbf{F}^*_{BB}[K,K]). \tag{17}$$

By introducing the auxiliary variable $\mathbf{z} \in \mathcal{R}^{K\times 1}$, we have $\mathbf{z}[i] = \mathbf{F}_{BB}[i,i]\mathbf{F}_{BB}[i,i]^H \geq 0$. Then, Eq. (15) is reformulated as

$$P_tN_t||\alpha_k^{[0]}\beta_k^{[0]}||^2\mathbf{z}[k] - \sum_{i\neq k}P_t\gamma_0P_{I,(i,k)}\mathbf{z}[i] = \sigma^2\gamma_0. \tag{18}$$

According to Eq. (18), Eq. (16) is further expressed as

$$\begin{cases}\mathbf{A}\mathbf{z} = \mathbf{b}\\ \sum_{i=1}^K \mathbf{z}(i) = P_t/||\mathbf{F}_{RF}||^2,\\ \mathbf{z}[i] \geq 0, \forall i = 1,2,\cdots,K,\end{cases} \tag{19}$$

where we have $\mathbf{b} = [\sigma^2\gamma_0,\sigma^2\gamma_0,\cdots,\sigma^2\gamma_0]$ and the matrix $\mathbf{A}$ is expressed as

$$\mathbf{A} = P_t\begin{bmatrix} N_t||\alpha_1^{[0]}\beta_1^{[0]}||^2 & \gamma_0P_{I,(2,1)} & \cdots & \gamma_0P_{I,(K,1)}\\ \gamma_0P_{I,(1,2)} & N_t||\alpha_2^{[0]}\beta_2^{[0]}||^2 & \cdots & \gamma_0P_{I,(2,K)}\\ \vdots & \vdots & \ddots & \vdots\\ \gamma_0P_{I,(1,K)} & \gamma_0P_{I,(2,K)} & \cdots & N_t||\alpha_K^{[0]}\beta_K^{[0]}||^2\end{bmatrix}. \tag{20}$$

Given a specific γ_0, Eq. (19) represents a linear-programming problem, which can be solved by a standard convex optimisation toolbox. Furthermore, a one-dimensional search is relied upon for obtaining the maximum γ_0, which is detailed in Algorithm 1.

Then, we analyze the complexity of our proposed Algorithm 1. Its main complexity lies in solving Eq. (19), which is a linear programing problem having K variables. Let I_0 denote the number of times a one-dimensional search has to be carried out. For a given accuracy tolerance ε, the computational complexity of obtaining $\mathbf{F}_{BB}$ is on the order of $O(\log_2(1/\varepsilon)I_0K^{2.5})$ according to [35]. Then the complexity of obtaining the analog TBF $\mathbf{F}_{RF}$ is $O(N_tK)$ according to *Proposition 1*. Thus, the overall complexity of Algorithm 1 is $O(N_tK+\log_2(1/\varepsilon)I_0K^{2.5})$.

Our hybrid TBF $\mathbf{F}^*_{RF}$ and $\mathbf{F}^*_{BB}$ is obtained in closed form at an extremely low complexity, which can be readily implemented in practice. The structure of our hybrid TBF indicates that we can increase the rate of the k-th user by simply improving the power of the corresponding RF chain, which only imposes limited interference on other users.

Algorithm 1 The Hybrid Beamforming Design in THz bands

Input: The channels $\{\mathbf{h}_i | i = 1, 2, \cdots, K\}$;
Output: The SINR γ_0, the hybrid TBF $\mathbf{F}_{RF}$ and $\mathbf{F}_{BB}$;
Initialise the upper bound γ_u, lower bound γ_l and γ_m
Obtain the analog TBF $\mathbf{F}_{RF}$ according to *Proposition 1*;
while $(\delta > \varepsilon)$ **do**
  Update $\gamma_m \leftarrow (\gamma_u + \gamma_l)/2$;
  Obtain $\mathbf{F}_{BB}$ by solving Eq. (19);
  if LP is feasible **then**
    Update $\gamma_l = \gamma_m$;
  else
    Update $\gamma_u = \gamma_m$;
  end if
  Calculate $\delta = \gamma_u - \gamma_l$;
end while
Return $\{\mathbf{F}_{RF}, \mathbf{F}_{BB}\}$

Remark 5: The increasing request and popularity of on-demand video and broadcast-like applications for smartphones has promoted an intensive area of research and standardization activities, under the terminology of LTE and 5G New Radio with multimedia broadcast/multicast service [36]. Recently, mainly due to the use of multiple antennas and the related signal-processing methods, physical-layer multicasting has been widely studied for implementing multicast communication at the physical layer of the network [37]. When we consider the multicast downlink, a transmitter sends the same signal and there is only a single information flow since a common message is delivered to a group of users. Then, we do not have any interference term in Eq. (8). We still maximize the minimum achievable rate of users. By adopting a similar optimal architecture and the asymptotically optimal condition, the hybrid TBF is derived in closed form as

$$\begin{aligned}
&\mathbf{F}^*_{RF} = [\mathbf{a}_t(\theta_1^{[0]}, \phi_1^{[0]})^H, \mathbf{a}_t(\theta_2^{[0]}, \phi_2^{[0]})^H, \cdots, \mathbf{a}_t(\theta_K^{[0]}, \phi_K^{[0]})^H], \\
&\mathbf{F}^*_{BB}[k,k] = \frac{\sqrt{P_t}}{(\alpha_k^{[0]}\beta_k^{[0]})^2 \sqrt{\left(\sum_{i=1}^{K} \frac{1}{(\alpha_i^{[0]}\beta_i^{[0]})^2}\right)}}, \\
&\quad \forall k \in \{1, 2, \cdots, K\}.
\end{aligned} \tag{21}$$

IV. Hybrid Beamforming Design in Multi-carrier Multi-user System

A. System Model

The system consists of a single transmitter and K users, while it has M sub-carriers. All the users are equipped with a single RA, while the transmitter is equipped with a very large number N_t of TAs. Moreover, N_{RF} RF chains are used at the transmitter, which satisfies $1 \le K \le N_t$. The transmitter sends modulated symbols s_m at the m-th sub-carrier to the k-th user, where $s_m \sim \mathcal{CN}(0, 1)$ is a complex random scalar.

The baseband digital TBF $\mathbf{f}_{BB,m} \in \mathbb{C}^{K\times 1}$ converts the modulated symbols to K RF chains at the m-th sub-carrier. Then the passband analog TBF $\mathbf{F}_{RF} \in \mathbb{C}^{N_t \times K}$ forwards the output of the K RF chains to the N_t TAs for transmission. A full-connection topology is used between the RF chains and the TAs. Note that the analog TBF is constituted by a number of analog phase-shifters satisfying $\|\mathbf{F}_{RF}(i, j)\| = 1, \forall i, \forall j$. The transmit signal at the m-th sub-carrier is then expressed as $\mathbf{x}_m = \mathbf{F}_{RF}\mathbf{f}_{BB,m}\mathbf{s}_m$. The signal received by the k-th user at the m-th sub-carrier is obtained as

$$y_k[m] = \mathbf{h}_{k,m}\mathbf{F}_{RF}\mathbf{f}_{BB,m}\mathbf{s}_m + n_k, \tag{22}$$

for $\forall k = 1, 2, \cdots, K$, where the complex random scalar $n_{k,m}$ represents the Gaussian noise at the user. The $N_t \times 1$ complex vector $\mathbf{h}_{k,m}$ is the channel directed towards the k-th user at the m-th sub-carrier.

Based on the received signal of the k-th user at the m-th sub-carrier expressed in Eq.(7), the SNR of the k-th user at the m-th sub-carrier is formulated as

$$\gamma_{k,m} = \frac{\|\mathbf{h}_{k,m}\mathbf{F}_{\mathbf{RF}}\mathbf{f}_{\mathbf{BB,m}}[:, k]\|^2}{\sigma_m^2}. \tag{23}$$

upon denoting the set of sub-carriers allocated to the k-th user by $\mathcal{M}_k = \{m_{k_1}, m_{k_2}, \cdots, m_{k_j}\}$, the symbol $\mathbf{s}_k$ for the k-th user is modulated to $|\mathcal{M}_k|$ subcarriers, i.e., $|\mathcal{M}_k|$ subcarriers serve the k-th user and every subcarrier passes through K RF chains. Then the achievable rate of the k-th user is expressed as

$$R_k = \sum_{i\in\mathcal{M}_k} \log_2(1 + \gamma_{k,i}). \tag{24}$$

B. Channel Model

The channel model at the m-th sub-carrier is reformulated as

$$\begin{aligned}
\mathbf{h}(m) =& \alpha^{[0]} e^{j2\pi\tau_{m,0} f_m} \beta^{[0]} \mathbf{a}_t(\theta^{[0]}, \phi^{[0]}, m) \\
&+ \sum_{i=1}^{L} \alpha^{[i]}\beta^{[i]} e^{j2\pi\tau_{m,i} f_m} \mathbf{a}_t(\theta^{[i]}, \phi^{[i]}, m),
\end{aligned} \tag{25}$$

where the first term is the LoS component and the second summation term is the NLoS component, as shown in Fig. 1. Specifically, $\alpha^{[0]}$, $\beta^{[0]}$ and $\tau_{m,0}$ represent the channel's fading coefficient, the path-loss coefficient and time-delay of the LoS component, respectively. The NLoS component has L different propagation paths, while $\alpha^{[i]}$, $\beta^{[i]}$ and $\tau_{m,i}$ represent the channel's fading coefficient, the path-loss coefficient and the time-delay of the i-th path. The path-loss includes both the spreading loss and molecular absorption loss, which is given by [19]

$$|\beta|^2 = L_{\text{spr}}(f, d) L_{\text{abs}}(f, d) = \left(\frac{c}{4\pi f d}\right)^2 e^{-k_{\text{abs}}(f)d}. \tag{26}$$

Moreover, the channel response vector $\mathbf{a}_t(\theta^{[i]}, \phi^{[i]}, m)$ is expressed as

$$\begin{aligned}
&\mathbf{a}_t(\theta^{[i]}, \phi^{[0]}, m) \\
&= \frac{1}{\sqrt{N_t}} \left[1, \cdots, e^{j\frac{2\pi f_m}{c} d((W-1)\sin(\theta^{[i]})\sin(\phi^{[i]}) + (H-1)\cos(\phi^{[i]}))}\right],
\end{aligned} \tag{27}$$

where f_m is the center frequency of the m-th sub-carrier.

When we generate the analog beamformer $\frac{1}{\sqrt{N_t}}\left[1, \cdots, e^{j\frac{2\pi f_c}{c} d((W-1)\sin(\theta^{[i]})\sin(\phi^{[i]}) + (H-1)\cos(\phi^{[i]}))}\right]$, there exists a phase offset $e^{j2\pi(f_c - f m)}$ between the analog beamformer and the channel response vector, which is related to the carrier frequency. Therefore, the beams will point to different physical directions surrounding the target physical direction at different subcarriers [38]. This effect is termed as beam

split in THz communication. Furthermore, the multi-path transmission results in a time-delay between any two paths, which leads to a phase offset between the different paths at the same sub-carrier.

Remark 6: As revealed in [38], the phase offset of multi-carrier systems can be eliminated either by the true-time-delay, or by the RF chain. When we consider a THz channel which contains a strong LoS path, we only have to focus on the LoS time-delay at every carrier. Therefore, we can eliminate the phase offset in the digital domain by realizing the phase shift $e^{j[2\pi f_m \tau + 2\pi(f_c - fm)]}$ at every carrier. Therefore, we solve the beam split problem in the digital domain of the hybrid TBF.

C. Problem Formulation and Algorithm

We assume that every user is allocated M/K sub-carriers. We aim for maximizing the minimum rate of the multi-user system by jointly optimising the digital TBF $\mathbf{f}_{BB,1}, \cdots, \mathbf{f}_{BB,M}$ and the analog TBF $\mathbf{F}_{RF}$, which is formulated as

$$\text{(P2)}: \max_{\mathbf{f}_{BB,1},\cdots,\mathbf{f}_{BB,M},\mathbf{F}_{RF}} \min_{1\le k\le K} R_k, \tag{28}$$

$$\text{s. t. } \sum_{m=1}^{M} \|\mathbf{f}_{BB,m}\mathbf{F}_{RF}\|^2 = P_t, \tag{28a}$$

$$\|\mathbf{F}_{RF}[i,j]\|^2 = 1, \forall i, j. \tag{28b}$$

(P2) is equivalent to the following problem:

$$\text{(P3)}: \max_{\mathbf{f}_{BB,1},\cdots,\mathbf{f}_{BB,M},\mathbf{F}_{RF}} R_0, \tag{29}$$

$$\text{s. t. } R_k \ge R_0 \tag{29a}$$

$$\sum_{m=1}^{M} \|\mathbf{f}_{BB,m}\mathbf{F}_{RF}\|^2 = P_t, \tag{29b}$$

$$\|\mathbf{F}_{RF}[i,j]\|^2 = 1, \forall i, j. \tag{29c}$$

Proposition 6: The asymptotically optimal analog TBF is $\mathbf{F}^*_{RF} = [\mathbf{a}_t(\theta_1^{[0]}, \phi_1^{[0]})^H, \mathbf{a}_t(\theta_2^{[0]}, \phi_2^{[0]})^H, \cdots, \mathbf{a}_t(\theta_K^{[0]}, \phi_K^{[0]})^H]$, where $\mathbf{a}_t(\theta_k^{[0]}, \phi_k^{[0]})$ is the channel response vector in the LoS path directed towards the k-th user and $\theta_k^{[0]}$ ($\phi_k^{[0]}$) is the departure azimuth (elevation) angle in this path.

Proof 2: In the multi-carrier system, we still adjust the analog beamformer to target every user. By adopted the channel sparsity and orthogonality, we only need to focus on the LoS path. The proof is similar to the Appendix B.

Proposition 7: Given the asymptotically optimal analog TBF $\mathbf{F}^*_{RF}$, only the i-th element in the m-th sub-carrier allocated to the i-th user's asymptotically optimal digital TBF $\mathbf{f}^*_{BB,m}$ is non-zero.

Proof 3: Note that the i-th column of the optimal analog TBF $\mathbf{F}^*_{RF}$ is targeted at the i-th user. When the m-th sub-carrier is allocated to the i-th user, only the i-th element in the m-th sub-carrier allocated to the i-th user's asymptotically optimal digital TBF $\mathbf{f}^*_{BB,m}$ is non-zero. Otherwise, the transmitted beam is directed to other direction, which has no contribution to the i-th user. The proof is similar to that in Appendix C.

Proposition 8: Given the asymptotically optimal analog TBF $\mathbf{F}^*_{RF}$ in *Proposition 6* and the structure of the digital TBF $\{\mathbf{f}_{BB,1}, \cdots, \mathbf{f}_{BB,M}\}$ in *Proposition 7*, the asymptotically optimal solution of $\{\mathbf{f}_{BB,1}, \cdots, \mathbf{f}_{BB,M}\}$ is obtained when all the users have the same rate.

Proof 4: Assume that the optimal solution is expressed as $\{\mathbf{f}_{BB,1}, \cdots, \mathbf{f}_{BB,M}, \mathbf{F}_{RF}\}$, while the objective function is R_0 and the rate of the k-th R_k is higher than R_0. Let the auxiliary functions $R_k(\mathbf{f}_{BB,m}|m \in \mathcal{M}_k)$ represent the rate of the k-th user, where $\mathcal{M}_k$ is the sub-carrier set allocated to the k-th user. There exists a number $\rho \in [0,1]$ satisfying $R_k(\rho\mathbf{f}_{BB,m}|m \in \mathcal{M}_k) = R_0$, due to the positive correlation between the transmit power and the rate. Then we can always find a solution having a higher objective function value, which is expressed as

$$\begin{cases} \mathbf{f}'_{BB,m} = \mathbf{f}_{BB,m} + a, \ \forall m \notin \{m_k, \cdots, m_{k+i}\} \\ \mathbf{f}'_{BB,m} = \rho\mathbf{f}_{BB,m} + a, \ \forall m \in \{m_k, \cdots, m_{k+i}\}, \\ \mathbf{F}_{RF} = \mathbf{F}_{RF} \end{cases} \tag{30}$$

where a satisfies $\sum_{m=1}^{M} \|\mathbf{f}'_{BB,m}\mathbf{F}_{RF}\|^2 = 1$. Note that the achievable rate of all the users are larger than R_0, which results in a conflict. The proof is complete.

According to *Proposition 6-8*, we can solve (P3) by the following way: Given any R_0, we find the minimum transmit power for every user to satisfy R_0. If the sum-power of all the users is higher than P_t, we may reduce R_0; Otherwise, we increase R_0. Based on the bisection search, we can obtain the optimal R^*. The details are summarized in Algorithm 2.

Assume that the total power allocated to the k-th user is P_k. Then maximum rate of the user is obtained by solving the following problem

$$\text{(P4)}: \max_{\{\mathbf{f}_{BB,i}|i\in\mathcal{M}_i\},\mathbf{F}_{RF}} R_0, \tag{31}$$

$$\text{s. t. } \sum_{m\in\mathcal{M}_i} \|\mathbf{f}_{BB,m}\mathbf{F}_{RF}\|^2 = P_k, \tag{31a}$$

$$\|\mathbf{F}_{RF}[i,j]\|^2 = 1, \forall i, j. \tag{31b}$$

The optimal solution is expressed as

$$\mathbf{f}_{BB,m} = \begin{cases} e^{j\theta_m}\sqrt{1/\mu - N_0/\lambda^2}, \ 1/\mu - N_0/\lambda^2 \ge 0 \\ 0, \ else \end{cases} \tag{32}$$

where $\theta_m = 2\pi f_m \tau + 2\pi(f_c - fm)$ and $1/\mu$ satisfies $\sum_{m=1}^{M} \|\mathbf{f}_{BB,m}\mathbf{F}_{RF}\|^2 = P_t$.

Then, we analyze the complexity of Algorithm 2. Its main complexity lies in solving (P4) by the water-filling method. Let I_1 and I_2 denote the number of times a one-dimensional search for R_m and $P_{i,m}$ is carried out, respectively. The complexity of obtaining $\mathbf{f}_{BB}$ is $O(I_1 I_2 |\mathcal{M}|^2)$ according to [39]. Then the complexity of obtaining the analog TBF $\mathbf{F}_{RF}$ is $O(N_t K)$ according to *Proposition 1*. Thus, the overall complexity of the Algorithm is $O(N_t K + I_1 I_2 |\mathcal{M}|^2)$.

V. Numerical Results

The number of TAs is set to $N_t = 128 = 16 \times 8$, while every user is equipped with a single RA. The number of paths in Eq. (2) is set to 3 [20]. The path-loss of the NLoS component is 20 dB higher than that of the LoS component in Eq. (2) [20]. The noise power is set to $\sigma^2 = -75$ dBm, while the transmit power is set to $P_t = 30$ dBm. In the downlink broadcast system, we

Algorithm 2 The Multi-carrier Hybrid Beamforming Design in THz bands

Input: The channels $\{\mathbf{h}_i | i = 1, 2, \cdots, K\}$; Initialized R_0; The error ε;
Output: The hybrid TBF $\{\mathbf{f}_{BB,1}, \cdots, \mathbf{f}_{BB,M}, \mathbf{F}_{RF}\}$;

Initialise the upper bound R_u, lower bound R_l and R_m
Obtain the analog TBF $\mathbf{F}_{RF}$ according to *Proposition 1*;
while $(\delta_1 > \varepsilon)$ **do**
  Update $R_m \leftarrow (R_u + R_l)/2$;
  while $(\delta_2 > \varepsilon)$ **do**
    for $i = 1 : K$ **do**
      Initialise the upper bound $P_{i,u}$, lower bound $P_{i,l}$ and $P_{i,m}$.
      Update $P_{i,m} \leftarrow (P_{i,u} + P_{i,l})/2$;
      Obtain $\{\mathbf{f}_{BB,1}, \cdots, \mathbf{f}_{BB,M},\}$ by solving Eq. (19);
      if $R_i > R_0$ **then**
        Update $P_{i,l} = P_{i,m}$;
      else
        Update $P_{i,u} = P_{i,m}$;
      end if
      Calculate $\delta_2 = P_{i,u} - P_{i,l}$;
    end for
  end while
  if $\sum_{m=1}^{M} \|\mathbf{f}_{BB,m}\mathbf{F}_{RF}\|^2 > P_t$ **then**
    Update $R_l = R_m$;
  else
    Update $R_u = R_m$;
  end if
  Calculate $\delta_1 = R_u - R_l$;
end while
Return $\{\mathbf{f}_{BB,1}, \cdots, \mathbf{f}_{BB,M}, \mathbf{F}_{RF}\}$

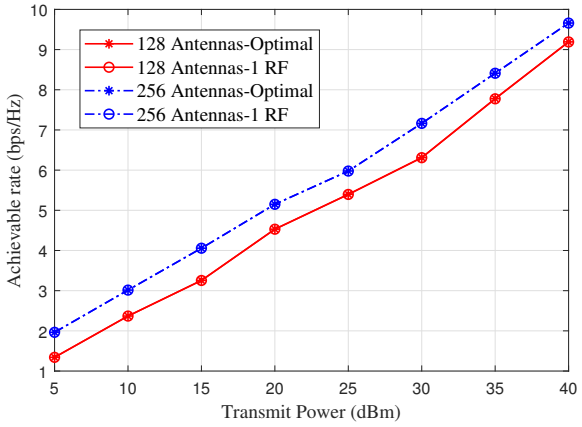

Fig. 4. Achievable rate of a single user in THz bands.

set the carrier frequency as 151 GHz and the distance from the transmitter to all the users as 5 m, the pass-loss is caculated according to Eq. (26). The maximum length of the plane is $D = 16 \times \frac{\lambda}{2} = 8\lambda$. Thus the radius of the near-field zone is $\frac{2D^2}{\lambda} = 128\lambda$, which is much lower than the distance from the users to the transmitter. Therefore, all the users in our systems are located in the far-field. Again, the rate per-user is defined as the minimum one among all the users.

A. Single-Carrier Single-User System in THz Bands

In Fig. 4, we first characterise the achievable rate of a single user in the THz band. The optimal TBF is the maximum-ratio TBF as mentioned in Section II, while the legend 1-RF represents our proposed single-RF hybrid TBF. Observe from Fig. 4 that our proposed hybrid TBF performs similarly to its optimal counterpart, because the path-loss of the LoS component is far lower than that of the NLoS components. We only have to focus the beam on the LoS components to achieve near-optimal performance. The numerical results confirm our *Proposition 2*.

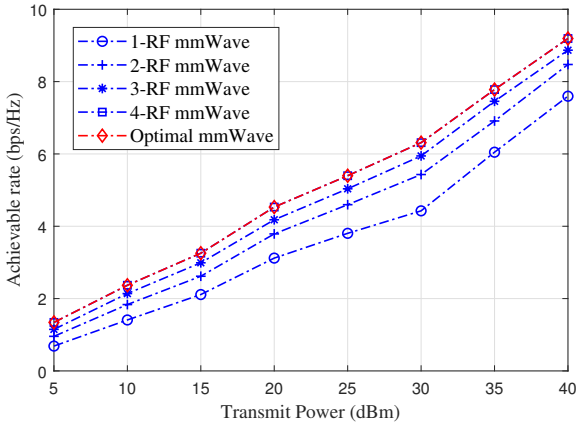

Fig. 5. Achievable rate of a single user in mmWave bands.

In Fig. 5, we also characterise the rate of a single user in the mmWave band. The mmWave channel is denoted as "mmWave", while the number of NLoS paths is also set to $L = 3$. Observe from Fig. 5 that the rate increases, as the transmitter has more RF chains. When the transmitter has 4 RF chains, it achieves the same rate as the optimal TBF. This is because the transmitter having 4 RF chains is capable of extracting the full channel gain from 4 paths, which also confirms our *Proposition 1* in Section II.

B. Single-Carrier Multi-User System in THz Bands

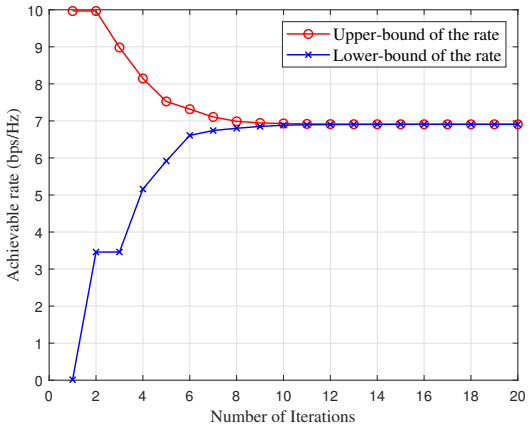

Fig. 6. Achievable rate vs number of iterations.

Let us now investigate the convergence of our proposed algorithm. The number of users is set to 3. Both the upper-bound and the lower-bound of the rate are introduced in Algorithm 1. Observe from Fig. 6 that in every iteration, the upper bound reduces, while the lower bound increases. Furthermore,

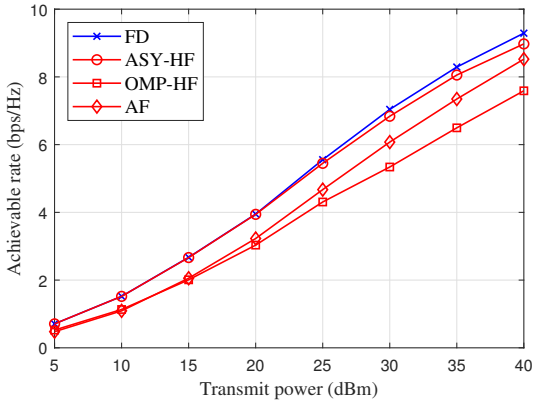

Fig. 7. Achievable rate vs transmit power.

our algorithm converges after 10 iterations. Moreover, we evaluate the impact of the transmit power on the rate in Fig. 7. The optimal full-digital TBF is denoted as “FD", while our proposed hybrid TBF, our proposed analog TBF and the orthogonal matching pursuit hybrid TBF [40] are denoted as “ASY-HF", “AF" and “OMP-HF", respectively. The optimal full-digital TBF is optimized by semi-definite programming (SDP), while the “OMP-HF" relies on this full-digital TBF. As expected, the rate increases as we increase the transmit power. When the transmit power is 20 dBm, the rate of “ASY-HF" is 3.94 bps/Hz. Furthermore, the rate of “ASY-HF" is close to that of the full-digital TBF, while it is 0.91 bps/Hz higher than that of “OMP-HF”. The rate of “ASY-HF" is also 0.71 bps/Hz higher than that of “AF". That is because the digital TBF relies on power allocation to achieve improved performance.

Let us now investigate the impact of the number of TAs on the rate in Fig. 8(a). The number of the users is set to 3, where the rate increases with the number of TAs due to the increased TBF gain. Specifically, the rate of our proposed "ASY-HF" increases by 1.15 bps/Hz as we increase the number of TAs from 128 to 256. We also observe that the rate gap between the "ASY-HF" and the "FD" solution is lower, when the number of TAs increases form 128 to 256, because the angular separation becomes more pronounced for more TAs. We also investigate the computing time of different algorithms in Fig. 8(b). The computer is equipped with an AMD Ryzen-5-3600 central processing unit (CPU) and 16 GByte random access memory (RAM). Observe from Fig. 8(b) that the computing time of "OMP-HF" is 29.5 times higher than that of our proposed "ASY-HF".

Next we investigate the impact of the path-loss ratio between the LoS component and the NLoS component on the rate in Fig. 9. The path-loss ratio is defined by $\frac{\beta^{[0]}}{\sum_{i=1}^{L}\beta^{[i]}}$. As shown in Fig. 9, the rate increases, when the path-loss ratio increases from 0 dB to 15 dB. This is because our "ASY-HF" design only considers the LoS component of the channel, while ignoring the NLoS components. When the path-loss ratio is low, the NLoS components become as important as the LoS components, while the lack of sufficient consideration for NLoS components degrades the performance of our design.

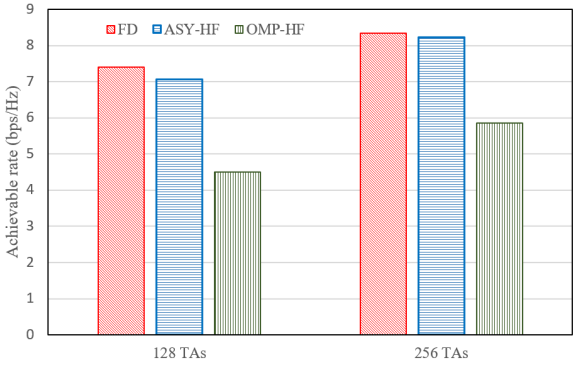

(a) Achievable rate vs number of TAs

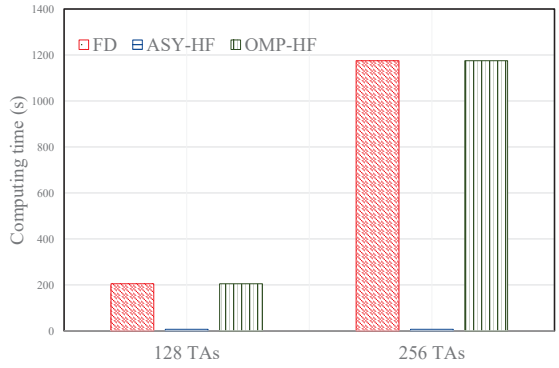

(b) Computing time

Fig. 8. Performance versus the number of TAs.

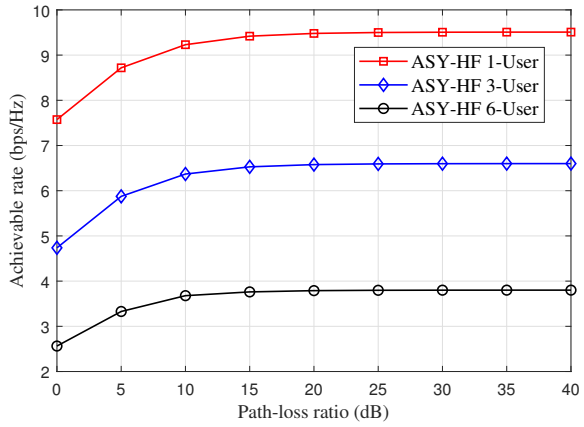

Fig. 9. Achievable rate vs the path-loss ratio between the LoS component and NLoS component.

As the path-loss ratio becomes higher, the LoS component becomes dominant. Our proposed TBF is asymptotically optimal according to *Proposition 3, 4 and 5*. Therefore, estimating the LoS component is sufficient for our design to achieve asymptotically optimal rate. As the path-loss ratio continues to increase, our joint design asymptotically approaches the optimal rate of 6.59 bps/Hz for 3 users. We also observe that the rate degrades, when we have more users. For example, it reduces by 2.91 bps/Hz, when we increase the number of users from 1 to 3. This is because the total transmit power is

shared by more users, which results in the reduction of the signal power of a single user. Furthermore, having more users results in increasing the interference.

C. Multi-Carrier single-User System in THz Bands

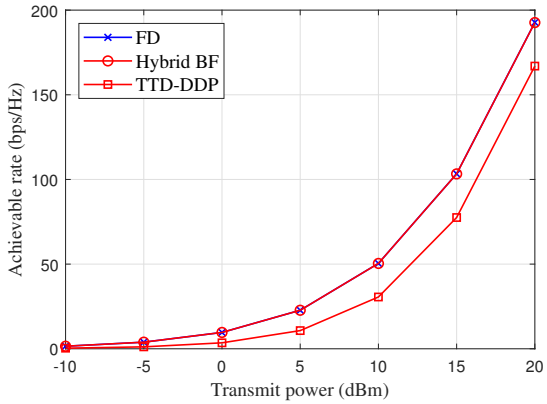

Fig. 10. Achievable rate in a multi-carrier system.

In multi-carrier system, the frequency range is set to 273-400 GHz, the bandwidth of each sub-carrier is 1 GHz, while the number of sub-carriers is set to 128. The molecular absorption coefficients are generated according to [41]. The noise power is set to -75 dBm [19]. The optimal full-digital TBF is denoted as "FD", which is the upper bound of the achievable rate. Our proposed hybrid TBF can be simplified to single-user situation by solving (P4) with the classic water-filling method. The true-time-delay based TBF [38] is denoted as "TTD-DDP", which uses time delay devices to solve the beam split problem. We investigate the impact of the transmit power on the achievable rate in Fig. 10. Observe from Fig. 10 that our hybrid beamformer performance is much better than the TTD-DDP and achieves almost the same rate as the upper bound. This is because the TTD-DDP has hardware limits of the time delay devices, while we treat the beam split in the digital domain.

D. Multi-Carrier Multi-User System in THz Bands

We investigate the impact of the transmit power on the rate in Fig. 11. The number of users is set to 4. Observe from Fig. 11 that our hybrid beamformer achieves almost the same rate as its full-digital counterpart. This is because we can eliminate the phase offset in the digital domain, which avoids the performance loss. This also confirms our theory detailed in Section IV.

VI. Conclusions

By exploiting the sparsity of THz channels, we demonstrated that a single RF chain is sufficient to ensure a near-optimal TBF design in single-carrier single-user systems, since we only have to adjust the phases of the transmit signals in the analog domain. Furthermore, we revealed the angular orthogonality of users, which substantially reduces

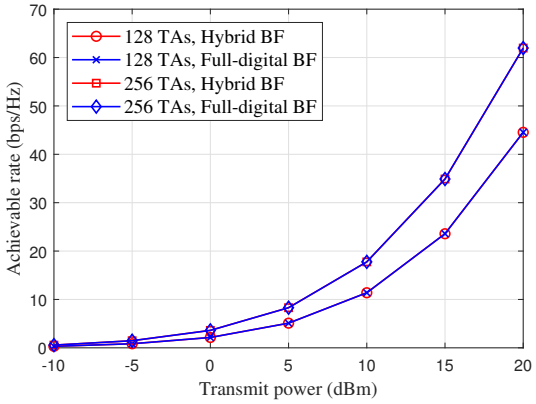

Fig. 11. Achievable rate in a multi-carrier system.

the complexity of obtaining an asymptotically optimal TBF design in single-carrier multi-user systems, and approaches the achievable rate of its SDP based full-digital counterpart. However, the computing time of the SDP based full-digital TBF is 29.5 times higher than that of our proposed hybrid TBF. Moreover, we derived the closed-form TBF design of multi-carrier multi-user systems by exploiting the angular orthogonality, ultimately resulting in the same performance as its full-digital counterpart.

Appendix A
Proof of Lemma 1

Since $\mathbf{a}_t(\theta_k^{[0]},\phi_k^{[0]})\mathbf{a}_t(\theta_k^{[0]},\phi_k^{[0]})^H = N_t$, we have

$$\lim_{N_t\to\infty}\frac{\mathbf{a}_t(\theta_k^{[0]},\phi_k^{[0]})\mathbf{a}_t(\theta_k^{[0]},\phi_k^{[0]})^H}{N_t} = \frac{N_t}{N_t} = 1. \tag{33}$$

Furthermore, the fraction of $\mathbf{a}_t(\theta_k^{[0]},\phi_k^{[0]})\mathbf{a}_t(\theta_{k'}^{[0]},\phi_{k'}^{[0]})^H/N_t$ can be derived in Eq.(33).

Since the channel's response vectors $\mathbf{h}_k$ and $\mathbf{h}_{k'}$ have different departure azimuth angles, we have $\theta_k^{[0]} \neq \theta_{k'}^{[0]}$ and $\phi_k^{[0]} \neq \phi_{k'}^{[0]}$. Therefore, the term $\mathrm{csc}(m\pi(\sin(\theta_k^{[0]})\sin(\phi_k^{[0]}) - \sin(\theta_{k'}^{[0]})\sin(\phi_{k'}^{[0]})) + n\pi(\cos(\phi_k^{[0]}) - \cos(\phi_{k'}^{[0]})))$ has a finite value. When the number of TAs tends to infinity, we have $\lim_{N_t\to\infty}\mathbf{a}_t(\theta_k^{[0]},\phi_k^{[0]})\mathbf{a}_t(\theta_{k'}^{[0]},\phi_{k'}^{[0]})^H/N_t = 0$.

Appendix B
Proof of Proposition 1

According to *Lemma 1*, $\{\mathbf{a}_t(\theta_1^{[0]},\phi_1^{[0]}),\mathbf{a}_t(\theta_2^{[0]},\phi_2^{[0]}),\cdots,\mathbf{a}_t(\theta_K^{[0]},\phi_K^{[0]})\}$ are asymptotically orthogonal to one another. We expand these K vectors to a group of orthogonal bases in a N_t-dimensional space, which is expressed as $\mathbf{A}_t = \{\mathbf{a}_t(\theta_1^{[0]},\phi_1^{[0]}),\mathbf{a}_t(\theta_2^{[0]},\phi_2^{[0]}),\cdots,\mathbf{a}_t(\theta_K^{[0]},\phi_K^{[0]}),\mathbf{a}_t(\theta_{K+1},\phi_{K+1}),\cdots,\mathbf{a}_t(\theta_{N_t},\phi_{N_t})\}$. Therefore, the analog TBF $\mathbf{F}_{RF}$ is a linear combination of these bases, which is expressed as

$$\mathbf{F}_{RF}^H = \mathbf{B}\mathbf{A}_t, \tag{35}$$

$$
\begin{aligned}
&\frac{\mathbf{a}_t(\theta_k^{[0]},\phi_k^{[0]})\mathbf{a}_t(\theta_{k'}^{[0]},\phi_{k'}^{[0]})^H}{N_t}\\
=&\frac{1}{N_t}\sum_{m=0}^{W-1}\sum_{n=0}^{H-1}\{[\cos(m\pi\sin(\theta_k^{[0]})\sin(\phi_k^{[0]})+n\pi\cos(\phi_k^{[0]}))+i\sin(m\pi\sin(\theta_k^{[0]})\sin(\phi_k^{[0]})+n\pi\cos(\phi_k^{[0]}))]\\
&\times[\cos(m\pi\sin(\theta_{k'}^{[0]})\sin(\phi_{k'}^{[0]})+n\pi\cos(\phi_{k'}^{[0]}))+i\sin(m\pi\sin(\theta_{k'}^{[0]})\sin(\phi_{k'}^{[0]})+n\pi\cos(\phi_{k'}^{[0]}))]^H\}\\
=&\frac{1}{N_t}\sum_{m=0}^{W-1}\sum_{n=0}^{H-1}\{\cos(m\pi\sin(\theta_k^{[0]})\sin(\phi_k^{[0]})+n\pi\cos(\phi_k^{[0]}))\cos(m\pi\sin(\theta_{k'}^{[0]})\sin(\phi_{k'}^{[0]})+n\pi\cos(\phi_{k'}^{[0]}))\\
&+\sin(m\pi\sin(\theta_k^{[0]})\sin(\phi_k^{[0]})+n\pi\cos(\phi_k^{[0]}))\sin(m\pi\sin(\theta_{k'}^{[0]})\sin(\phi_{k'}^{[0]})+n\pi\cos(\phi_{k'}^{[0]}))\\
&-i\cos(m\pi\sin(\theta_k^{[0]})\sin(\phi_k^{[0]})+n\pi\cos(\phi_k^{[0]}))\sin(m\pi\sin(\theta_{k'}^{[0]})\sin(\phi_{k'}^{[0]})+n\pi\cos(\phi_{k'}^{[0]}))\\
&+i sin(m\pi\sin(\theta_k^{[0]})\sin(\phi_k^{[0]})+n\pi\cos(\phi_k^{[0]}))\cos(m\pi\sin(\theta_{k'}^{[0]})\sin(\phi_{k'}^{[0]})+n\pi\cos(\phi_{k'}^{[0]}))\}\\
=&\frac{1}{N_t}\sum_{m=0}^{W-1}\sum_{n=0}^{H-1}\{\cos(m\pi(\sin(\theta_k^{[0]})\sin(\phi_k^{[0]})-\sin(\theta_{k'}^{[0]})\sin(\phi_{k'}^{[0]}))+n\pi(\cos(\phi_k^{[0]})-\cos(\phi_{k'}^{[0]})))\\
&+i\sin(m\pi(\sin(\theta_k^{[0]})\sin(\phi_k^{[0]})-\sin(\theta_{k'}^{[0]})\sin(\phi_{k'}^{[0]}))+n\pi(\cos(\phi_k^{[0]})-\cos(\phi_{k'}^{[0]})))\}\\
=&\frac{1}{N_t}(1+i)\csc(m\pi(\sin(\theta_k^{[0]})\sin(\phi_k^{[0]})-\sin(\theta_{k'}^{[0]})\sin(\phi_{k'}^{[0]}))+n\pi(\cos(\phi_k^{[0]})-\cos(\phi_{k'}^{[0]}))).
\end{aligned}
\tag{34}
$$

where $\mathbf{B}\in\mathbb{C}^{K\times N}$ contains all the array weights. Therefore, the i-th row of $\mathbf{F}_{RF}$ is expressed as

$$
\mathbf{F}_{RF}[i,:]^H=\sum_{j=1}^{K}\mathbf{B}[i,j]\mathbf{a}_t(\theta_j^{[0]},\phi_j^{[0]})+\sum_{n=K+1}^{N_t}\mathbf{B}[i,n]\mathbf{a}_t(\theta_n^{[0]},\phi_n^{[0]}).
\tag{36}
$$

The second summation term $\sum_{n=K+1}^{N_t}\mathbf{B}[i,n]\mathbf{a}_t(\theta_n,\phi_n^{[0]})$ has no contribution to any user due to the angular orthogonality, according to *Lemma 1*. Then we have $\mathbf{B}[i,n]=0,\ \forall n\in[K+1,\cdots,N_t]$. Eq. (36) is then reformulated as $\mathbf{F}_{RF}[i,:]^H=\sum_{j=1}^{K}\mathbf{B}[i,j]\mathbf{a}_t(\theta_j^{[0]},\phi_j^{[0]})$. Note that the analog TBF is realised by adjusting the phase-shifters. Therefore, the norm of the element at the i-th row and l-th column in $\mathbf{F}_{RF}$ should satisfy the following equality:

$$
\|\mathbf{F}_{RF}[i,l]\|^2=\|\sum_{j=1}^{K}\mathbf{B}[i,j]\mathbf{a}_t(\theta_l^{[0]},\phi_l^{[0]})[j]\|^2=1,\ \forall i,l,
\tag{37}
$$

where we have $\|\mathbf{a}_t(\theta_l^{[0]},\phi_l^{[0]})[j]\|=1$ according to Eq. (1). Unfortunately, it is difficult to obtain the weight matrix $\mathbf{B}$ from Eq. (37) due to its non-linearity. However, by considering $\|\mathbf{a}_t(\theta_l^{[0]},\phi_l^{[0]})[j]\|=1$, we can obtain a general solution to the weight matrix $\mathbf{B}$, which is expressed as

$$
\begin{cases}\mathbf{B}[i,j]=1 & i=j,j=1,2,\cdots,K.\\ \mathbf{B}[i,j]=0 & else.\end{cases}
\tag{38}
$$

As a result, the asymptotically optimal analog TBF is $\mathbf{F}_{RF}=[\mathbf{a}_t(\theta_1^{[0]},\phi_1^{[0]}),\mathbf{a}_t(\theta_2^{[0]},\phi_2^{[0]}),\cdots,\mathbf{a}_t(\theta_K^{[0]},\phi_K^{[0]})]$.

Appendix C
Proof of Proposition 3

According to the received signal y_k of Eq. (7), the SINR of the k-th user is formulated as

$$
\gamma_k=\frac{\frac{P_t\|\mathbf{h}_k\mathbf{F}_{\mathbf{RF}}\mathbf{F}_{\mathbf{BB}}[:,k]\|^2}{N_t}}{\frac{P_t\|\sum_{i\neq k}\mathbf{h}_k\mathbf{F}_{\mathbf{RF}}\mathbf{F}_{\mathbf{BB}}[:,i]\|^2}{N_t}+\frac{\sigma^2}{N_t}},
\tag{39}
$$

where $\mathbf{h}_k=\alpha_k^{[0]}\beta_k^{[0]}\mathbf{a}_t(\theta_k^{[0]},\phi_k^{[0]})+\sum_{i=1}^{L}\alpha_k^{[i]}\beta_k^{[i]}\mathbf{a}_t(\theta_k^{[i]},\phi_k^{[i]})$ is the channel response vector of the k-th user. When we adopt the asymptotically optimal analog TBF $\mathbf{F}_{RF}=[\mathbf{a}_t(\theta_1^{[0]},\phi_1^{[0]}),\mathbf{a}_t(\theta_2^{[0]},\phi_2^{[0]}),\cdots,\mathbf{a}_t(\theta_K^{[0]},\phi_K^{[0]})]$ of *Proposition 1*, we have

$$
\begin{aligned}
&\lim_{N_t\to\infty}\frac{\mathbf{h}_k\mathbf{F}_{\mathbf{RF}}}{N_t}\\
=&\lim_{N_t\to\infty}\frac{\mathbf{h}_k[\mathbf{a}_t(\theta_1^{[0]},\phi_1^{[0]}),\cdots,\mathbf{a}_t(\theta_k^{[0]},\phi_k^{[0]}),\cdots,\mathbf{a}_t(\theta_K^{[0]},\phi_K^{[0]})]}{N_t}\\
=&\lim_{N_t\to\infty}\frac{[\alpha_k^{[0]}\beta_k^{[0]}\mathbf{a}_t(\theta_k^{[0]},\phi_k^{[0]})+\sum_{i=1}^{L}\alpha_k^{[i]}\beta_k^{[i]}\mathbf{a}_t(\theta_k^{[i]},\phi_k^{[i]})]^T}{N_t}\\
&\times[\mathbf{a}_t(\theta_1^{[0]},\phi_1^{[0]}),\mathbf{a}_t(\theta_2^{[0]},\phi_2^{[0]}),\cdots,\mathbf{a}_t(\theta_K^{[0]},\phi_K^{[0]})]\\
=&[0,0,\cdots,\alpha_k^{[0]}\beta_k^{[0]},\cdots,0].
\end{aligned}
\tag{40}
$$

By substituting Eq. (40) into Eq. (39), the asymptotic SINR of the k-th user is expressed as

$$
\lim_{N_t\to\infty}\gamma_k=\frac{P_tN_t\|\alpha_k^{[0]}\beta_k^{[0]}\mathbf{h}_k\mathbf{a}_t(\theta_k^{[0]},\phi_k^{[0]})^H\mathbf{F}_{BB}[k,k]\|^2}{P_t\|\sum_{i\neq k}\mathbf{h}_k\mathbf{F}_{\mathbf{RF}}\mathbf{F}_{\mathbf{BB}}[:,i]\|^2+\sigma^2}.
\tag{41}
$$

Observe from Eq. (41) that $\mathbf{F}_{\mathbf{BB}}[k,k]$ is in the numerator, which contributes to the desired signal of the k-th user. $\{\mathbf{F}_{\mathbf{BB}}[k,i]|\forall i\neq k\}$ has no contributions to the k-th user, but it may increase the interference imposed on other users.

In order to maximize the SINR of the k-th user, we should simultaneously strengthen the desired signal and suppress the

interference. To this end, $\mathbf{F}_{BB}$ can be expressed as

$$\begin{cases}\mathbf{F}_{BB}[i,j] \neq 0 & i = j,\\ \mathbf{F}_{BB}[i,j] = 0 & \forall i \neq j.\end{cases} \tag{42}$$

As a result, $\mathbf{F}_{BB}$ has non-zero elements in its diagonal.

Appendix D
Proof of Proposition 4

Without loss of generality, we let the i-th user have the lowest SINR, while letting the k-th user have the highest SINR. Then, we have

$$\gamma_i < \gamma_j, \forall\, j \neq i,\, j \in \{1, 2, \cdots, K\}. \tag{43}$$

According to Eq. (15b), the asymptotical SINR of the i-th user is a function of $\mathbf{F}_{BB}[i,i]$ and $\mathbf{F}_{BB}[k,k]$, which can be expressed as

$$\gamma_i(\mathbf{F}_{BB}[i,i], \mathbf{F}_{BB}[k,k]) = \frac{P_t N_t \|\alpha_i^{[0]}\beta_i^{[0]}\mathbf{F}_{BB}[i,i]\|^2}{\sum_{j\neq i,k} P_{I,(j,i)}\|\mathbf{F}_{BB}[j,j]\|^2 + P_{I,(k,i)}\|\mathbf{F}_{BB}[k,k]\|^2 + \sigma^2}. \tag{44}$$

In order to obtain a higher fair SINR for the entire system, we may reduce the highest SINR of the k-th user and allocate higher power to the i-th user. In this way, we obtain a new solution achieving a higher fair SINR by following the process formulated below:

$$\begin{aligned}&\mathbf{F}'_{RF} = \mathbf{F}_{RF}\\ &\mathbf{F}'_{BB}[j,j] = \mathbf{F}_{BB}[j,j], \forall\, j \neq i,k\\ &\gamma_i(\mathbf{F}'_{BB}[i,i], \mathbf{F}'_{BB}[k,k]) = \gamma_k(\mathbf{F}'_{BB}[i,i], \mathbf{F}'_{BB}[k,k]).\end{aligned} \tag{45}$$

By solving Eq. (45), we can obtain a new solution, whose minimum SINR $\gamma' = \min\{\gamma'_1, \gamma'_2, \cdots, \gamma'_K\}$ is higher than that of the original one.

If there still exists a user, whose SINR is lower than that of the others in this new solution, we can repeat the above process to obtain a better solution. Finally, the solution converges to a situation that all the users have the same SINR.

References

[1] P. Yadav and S. Vishwakarma, "Application of internet of things and big data towards a smart city," in *Proc. 2018 3rd International Conference On Internet of Things: Smart Innovation and Usages (IoT-SIU)*, Bhimtal, India, Feb. 2018, pp. 1–5.

[2] Z. Chen, C. Han, Y. Wu, L. Li, C. Huang, Z. Zhang, G. Wang, and W. Tong, "Terahertz wireless communications for 2030 and beyond: A cutting-edge frontier," *IEEE Communications Magazine*, vol. 59, no. 11, pp. 66–72, Nov. 2021.

[3] I. F. Akyildiz, C. Han, Z. Hu, S. Nie, and J. M. Jornet, "Terahertz band communication: An old problem revisited and research directions for the next decade," *IEEE Transactions on Communications*, vol. 70, no. 6, pp. 4250–4285, Jun. 2022.

[4] C.-X. Wang, J. Wang, S. Hu, Z. H. Jiang, J. Tao, and F. Yan, "Key technologies in 6G terahertz wireless communication systems: A survey," *IEEE Vehicular Technology Magazine*, vol. 16, no. 4, pp. 27–37, Dec. 2021.

[5] L. Liu, J. L. Hesler, H. Xu, A. W. Lichtenberger, and R. M. Weikle, "A broadband quasi-optical Terahertz detector utilizing a zero bias schottky diode," *IEEE Microwave and Wireless Components Letters*, vol. 20, no. 9, pp. 504–506, Sep. 2010.

[6] F. Gao, B. Wang, C. Xing, J. An, and G. Y. Li, "Wideband beamforming for hybrid massive MIMO Terahertz communications," *IEEE Journal on Selected Areas in Communications*, vol. 39, no. 6, pp. 1725–1740, Jun. 2021.

[7] H. Ren, K. Wang, and C. Pan, "Intelligent reflecting surface-aided urllc in a factory automation scenario," *IEEE Transactions on Communications*, vol. 70, no. 1, pp. 707–723, Jan. 2022.

[8] E. Bjornson, L. Van der Perre, S. Buzzi, and E. G. Larsson, "Massive MIMO in sub-6G THz and mmwave: Physical, practical, and use-case differences," *IEEE Wireless Communications*, vol. 26, no. 2, pp. 100–108, Apr. 2019.

[9] A. F. Molisch, V. V. Ratnam, S. Han, Z. Li, S. L. H. Nguyen, L. Li, and K. Haneda, "Hybrid beamforming for massive MIMO: A survey," *IEEE Communications Magazine*, vol. 55, no. 9, pp. 134–141, Sep. 2017.

[10] C. Lin and G. Y. Li, "Energy-efficient design of indoor mmwave and sub-THz systems with antenna arrays," *IEEE Transactions on Wireless Communications*, vol. 15, no. 7, pp. 4660–4672, Jul. 2016.

[11] S. H. A. Shah, S. Aditya, and S. Rangan, "Power-efficient beam tracking during connected mode DRX in mmwave and sub-THz systems," *IEEE Journal on Selected Areas in Communications*, vol. 39, no. 6, pp. 1711–1724, Jun. 2021.

[12] H. Sarieddeen, M.-S. Alouini, and T. Y. Al-Naffouri, "Terahertz-band ultra-massive spatial modulation MIMO," *IEEE Journal on Selected Areas in Communications*, vol. 37, no. 9, pp. 2040–2052, Sep. 2019.

[13] S. K. Moorthy and Z. Guan, "Beam learning in mmwave/thz-band drone networks under in-flight mobility uncertainties," *IEEE Transactions on Mobile Computing*, vol. 21, no. 6, pp. 1945–1957, Jun. 2022.

[14] M. A. Almasi, L. Jiang, H. Jafarkhani, and H. Mehrpouyan, "Joint beamwidth and power optimization in mmwave hybrid beamforming-NOMA systems," *IEEE Transactions on Wireless Communications*, vol. 20, no. 4, pp. 2442–2456, Apr. 2021.

[15] H. Iimori, G. T. F. De Abreu, O. Taghizadeh, R.-A. Stoica, T. Hara, and K. Ishibashi, "A stochastic gradient descent approach for hybrid mmwave beamforming with blockage and CSI-error robustness," *IEEE Access*, vol. 9, pp. 74 471–74 487, May 2021.

[16] T. Van Le and K. Lee, "Adaptive perturbation-aided opportunistic hybrid beamforming for mmwave systems," *IEEE Transactions on Vehicular Technology*, vol. 69, no. 6, pp. 6554–6562, Jun. 2020.

[17] L. Zhao, M. Li, C. Liu, S. V. Hanly, I. B. Collings, and P. A. Whiting, "Energy efficient hybrid beamforming for multi-user millimeter wave communication with low-resolution A/D at transceivers," *IEEE Journal on Selected Areas in Communications*, vol. 38, no. 9, pp. 2142–2155, Sep. 2020.

[18] L. Zhu, J. Zhang, Z. Xiao, X. Cao, D. O. Wu, and X.-G. Xia, "Millimeter-wave NOMA with user grouping, power allocation and hybrid beamforming," *IEEE Transactions on Wireless Communications*, vol. 18, no. 11, pp. 5065–5079, Nov. 2019.

[19] H. Yuan, N. Yang, K. Yang, C. Han, and J. An, "Hybrid beamforming for Terahertz multi-carrier systems over frequency selective fading," *IEEE Transactions on Communications*, vol. 68, no. 10, pp. 6186–6199, Oct. 2020.

[20] C. Lin and G. Y. Li, "Adaptive beamforming with resource allocation for distance-aware multi-user indoor Terahertz communications," *IEEE Transactions on Communications*, vol. 63, no. 8, pp. 2985–2995, Aug. 2015.

[21] H. Li, M. Li, Q. Liu, and A. L. Swindlehurst, "Dynamic hybrid beamforming with low-resolution PSs for wideband mmwave MIMO-OFDM systems," *IEEE Journal on Selected Areas in Communications*, vol. 38, no. 9, pp. 2168–2181, Sep. 2020.

[22] C. Feng, W. Shen, J. An, and L. Hanzo, "Joint hybrid and passive ris-assisted beamforming for mmwave MIMO systems relying on dynamically configured subarrays," *IEEE Internet of Things Journal*, pp. 1–1, Aug. 2022.

[23] L. Pang, W. Wu, Y. Zhang, Y. Yuan, Y. Chen, A. Wang, and J. Li, "Joint power allocation and hybrid beamforming for downlink mmwave-NOMA systems," *IEEE Transactions on Vehicular Technology*, vol. 70, no. 10, pp. 10 173–10 184, Oct. 2021.

[24] J. Zhan and X. Dong, "Interference cancellation aided hybrid beamforming for mmwave multi-user massive MIMO systems," *IEEE Transactions on Vehicular Technology*, vol. 70, no. 3, pp. 2322–2336, Mar. 2021.

[25] C. Lin, G. Y. Li, and L. Wang, "Subarray-based coordinated beamforming training for mmwave and sub-THz communications," *IEEE Journal on Selected Areas in Communications*, vol. 35, no. 9, pp. 2115–2126, Sep. 2017.

[26] S. A. Busari, K. M. S. Huq, S. Mumtaz, J. Rodriguez, Y. Fang, D. C. Sicker, S. Al-Rubaye, and A. Tsourdos, "Generalized hybrid beamforming for vehicular connectivity using THz massive MIMO," *IEEE Transactions on Vehicular Technology*, vol. 68, no. 9, pp. 8372–8383, Sep. 2019.

[27] C. Lin and G. Y. Li, "Indoor Terahertz communications: How many antenna arrays are needed?" *IEEE Transactions on Wireless Communications*, vol. 14, no. 6, pp. 3097–3107, Jun. 2015.

[28] J. Qiao and M.-S. Alouini, "Secure transmission for intelligent reflecting surface-assisted mmwave and Terahertz systems," *IEEE Wireless Communications Letters*, vol. 9, no. 10, pp. 1743–1747, Oct. 2020.

[29] P. Wang, J. Fang, W. Zhang, and H. Li, "Fast beam training and alignment for IRS-assisted millimeter wave/Terahertz systems," *IEEE Transactions on Wireless Communications*, pp. 1–1, Apr. 2021.

[30] L. Yan, C. Han, and J. Yuan, "Energy-efficient dynamic-subarray with fixed true-time-delay design for terahertz wideband hybrid beamforming," *IEEE Journal on Selected Areas in Communications*, vol. 40, no. 10, pp. 2840–2854, Oct. 2022.

[31] H. Yuan, N. Yang, X. Ding, C. Han, K. Yang, and J. An, "Cluster-based multi-carrier hybrid beamforming for massive device terahertz communications," *IEEE Transactions on Communications*, vol. 70, no. 5, pp. 3407–3420, May 2022.

[32] B. Ning, Z. Chen, W. Chen, Y. Du, and J. Fang, "Terahertz multi-user massive MIMO with intelligent reflecting surface: Beam training and hybrid beamforming," *IEEE Transactions on Vehicular Technology*, vol. 70, no. 2, pp. 1376–1393, Feb. 2021.

[33] J. Qiao, C. Zhang, A. Dong, J. Bian, and M.-S. Alouini, "Securing intelligent reflecting surface assisted terahertz systems," *IEEE Transactions on Vehicular Technology*, vol. 71, no. 8, pp. 8519–8533, Aug. 2022.

[34] T. L. Marzetta, "Noncooperative cellular wireless with unlimited numbers of base station antennas," *IEEE Transactions on Wireless Communications*, vol. 9, no. 11, pp. 3590–3600, Nov. 2010.

[35] Y. T. Lee and A. Sidford, "Efficient inverse maintenance and faster algorithms for linear programming," in *Proceedings of the 2015 IEEE 56th Annual Symposium on Foundations of Computer Science (FOCS)*, ser. FOCS '15. USA: IEEE Computer Society, Oct. 2015, pp. 230–249. [Online]. Available: https://doi.org/10.1109/FOCS.2015.23

[36] E. Garro, M. Fuentes, J. L. Carcel, H. Chen, D. Mi, F. Tesema, J. J. Gimenez, and D. Gomez-Barquero, "5G mixed mode: NR multicast-broadcast services," *IEEE Transactions on Broadcasting*, vol. 66, no. 2, pp. 390–403, Jun. 2020.

[37] Y. Lee, "Multiobjective optimization for intelligent reflective surface-aided physical-layer multicasting," *IEEE Open Journal of the Communications Society*, vol. 3, pp. 411–423, Mar. 2022.

[38] L. Dai, J. Tan, Z. Chen, and H. V. Poor, "Delay-phase precoding for wideband THz massive MIMO," *IEEE Transactions on Wireless Communications*, vol. 21, no. 9, pp. 7271–7286, Sep. 2022.

[39] P. He, L. Zhao, S. Zhou, and Z. Niu, "Water-filling: A geometric approach and its application to solve generalized radio resource allocation problems," *IEEE Transactions on Wireless Communications*, vol. 12, no. 7, pp. 3637–3647, Jul. 2013.

[40] O. E. Ayach, S. Rajagopal, S. Abu-Surra, Z. Pi, and R. W. Heath, "Spatially sparse precoding in millimeter wave MIMO systems," *IEEE Transactions on Wireless Communications*, vol. 13, no. 3, pp. 1499–1513, Mar. 2014.

[41] A.-A. A. Boulogeorgos, E. N. Papasotiriou, and A. Alexiou, "A distance and bandwidth dependent adaptive modulation scheme for thz communications," in *Proc. 2018 IEEE 19th International Workshop on Signal Processing Advances in Wireless Communications (SPAWC)*, Kalamata, Greece, Jun. 2018, pp. 1–5.